Journal of Materials Chemistry A

PAPER

View Article Online
View Journal | View Issue

Cite this: J. Mater. Chem. A, 2018, 6, 5836

Computer simulations of 4240 MOF membranes for H_2/CH_4 separations: insights into structure–performance relations†

Cigdem Altintas,‡[a] Gokay Avci,‡[a] Hilal Daglar,‡[a] Ezgi Gulcay-Ozcan,‡[b] Ilknur Erucar *[c] and Seda Keskin *[a]

Design of new membranes having high H_2/CH_4 selectivity and high H_2 permeability is strongly desired to reduce the energy demand for H_2 production. Metal organic frameworks (MOFs) offer a great promise for membrane-based gas separations due to their tunable physical and chemical properties. We performed a high-throughput computational screening study to examine membrane-based H_2/CH_4 separation potentials of 4240 MOFs. Grand canonical Monte Carlo (GCMC) and molecular dynamics (MD) simulations were used to compute adsorption and diffusion of H_2 and CH_4 in MOFs. Simulation results were then used to predict adsorption selectivity, diffusion selectivity, gas permeability and membrane selectivity of MOFs. A large number of MOF membranes was found to outperform traditional polymer and zeolite membranes by exceeding the Robeson's upper bound for selective separation of H_2 from CH_4. Structure–performance analysis was carried out to understand the relations between MOF membranes' selectivities and their pore sizes, surface areas, porosities, densities, lattice systems, and metal types. Results showed that MOFs with pore limiting diameters between 3.8 and 6 Å, the largest cavity diameters between 6 and 12 Å, surface areas less than 1000 $m^2\ g^{-1}$, porosities between 0.5 and 0.75, and densities between 1 and 1.5 g cm^{-3} are the most promising membranes leading to H_2 selectivities >10 and H_2 permeabilities $>10^4$ Barrer. Our results suggest that monoclinic MOFs having copper metals are the best membrane candidates for H_2/CH_4 separations. This study represents the first high-throughput computational screening of the most recent MOF database for membrane-based H_2/CH_4 separation and microscopic insight provided from molecular simulations will be highly useful for the future design of new MOFs having extraordinarily high H_2 selectivities.

Received 13th February 2018
Accepted 20th February 2018

DOI: 10.1039/c8ta01547c

rsc.li/materials-a

1. Introduction

Metal organic frameworks (MOFs) are composed of metal complexes that are linked by organic ligands to create highly porous frameworks.[1,2] They have been recently considered as strong alternatives to traditional porous materials such as zeolites and activated carbons due to their attractive physical and chemical properties. MOFs offer very large surface areas (500–6500 $m^2\ g^{-1}$), high pore volumes (1–4 $cm^3\ g^{-1}$), wide range of pore sizes (1–98 Å), reasonable chemical and mechanical stabilities. The greatest advantage of MOFs over conventional porous materials is the ability to change the metal and organic linker combination during synthesis in order to create a large diversity of materials with different geometry, pore size and chemical functionality.[3,4] MOFs have been widely examined for a variety of physical, chemical and biological applications including gas storage,[5] gas separation,[6,7] drug storage and drug delivery,[8] catalysis,[9] optical and luminescent applications.[10] Among these, MOFs have received significant interest for adsorption-based and membrane-based gas separations due to their permanent porosities and tunable pore sizes.

[a]Department of Chemical and Biological Engineering, Koc University, Rumelifeneri Yolu, Sariyer, Istanbul, 34450, Turkey. E-mail: skeskin@ku.edu.tr; Tel: +90 212 338 1362

[b]Department of Mechanical Engineering, Faculty of Engineering, Ozyegin University, Cekmekoy, Istanbul, 34794, Turkey

[c]Department of Natural and Mathematical Sciences, Faculty of Engineering, Ozyegin University, Cekmekoy, Istanbul, 34794, Turkey. E-mail: ilknur.erucar@ozyegin.edu.tr; Tel: +90 216 564 9297

† Electronic supplementary information (ESI) available: Supporting data associated with this article can be found in the online version: comparison of our results and experiments for single-component and mixture gas permeances through various MOF membranes; relations between Henry's constants, diffusivities, permeabilities, adsorption selectivities, diffusion selectivities, membrane selectivities and PLD, LCD, SA, ϕ, ρ of MOFs; similarity indexes and unit cell representations of the top ten promising MOFs; comparison of $S^0_{ads,CH_4/H_2}$ with $S^{mix}_{ads,CH_4/H_2}$; comparison of the single-component and mixture calculations for the permeability and selectivities of the top promising MOF membranes. See DOI: 10.1039/c8ta01547c

‡ Equal contribution.

Continuous operation of membranes generates significant advantages compared to the more complex modes of operation needed for adsorption-based gas separation methods. Although a large number of experimental studies investigated adsorption-based gas separations with MOFs,[11] the number of studies on membrane-based gas separations using MOFs is limited due to the experimental challenges in making defect-free membranes from new crystalline materials.[12] We reviewed the literature on MOF membranes and showed that only 29 different types of MOF membranes were experimentally fabricated and tested for gas separations.[13] These MOF membranes were reported to have very good gas separation performances, higher selectivities and higher permeabilities, compared to the traditional polymer and zeolite membranes.[14] The number of synthesized MOF membranes has been increasing but most of the membranes were fabricated using the same materials, generally prototype MOFs, such as MOF-5,[15–19] CuBTC,[20–22] ZIF-8.[23–25] Considering the fact that the number of available MOFs has already reached to several thousands,[26] it is highly possible that there are many other materials with better gas separation performances but these MOFs have not been fabricated and tested as membranes yet. The large materials space creates an opportunity for the discovery of highly useful membrane candidates for target gas separations. On the other hand, it is not possible to fabricate and test thousands of MOF membranes using purely experimental manners at the lab scale.

Computational methods, specifically molecular simulations, play an important role in screening large number of MOFs for a target application in a time effective manner. Potential of molecular simulations in choosing the best MOFs for a given gas separation has been shown in several studies.[27] These simulations also provide molecular-level insights that can guide the experiments for design of new materials with better separation performances. Although molecular simulations have been widely used to examine CO_2/CH_4 and CO_2/N_2 separation performances of MOFs,[27–30] H_2/CH_4 separation is rarely investigated as we will discuss below. H_2/CH_4 separation is industrially important in the process of purification of synthesis gas obtained from steam reforming of natural gas. Hydrogen is an important chemical in many applications and its production depends on the decomposition of CH_4. Therefore, separation of H_2 from CH_4 with high selectivity and high permeability is strongly desired. Several different types of membrane materials such as zeolites[31] and polymers[32] have been studied for membrane-based separation of H_2/CH_4 mixtures in the past. However, these membranes could not meet the requirements of high H_2 selectivity and high H_2 permeability.[33]

Due to the tunability of pore sizes and shapes by judicious selection of metal clusters and organic linkers, MOFs offer great promise for efficient H_2/CH_4 separations. A small number of MOFs, maximum of 20, was studied using molecular simulations for membrane-based H_2/CH_4 separations in the literature.[27,34–38] Haldoupis *et al.*[39] performed the first large-scale molecular simulation study and used a geometric approach to calculate the ideal H_2/CH_4 selectivity of 143 MOF membranes at infinite dilution condition. They showed that many MOFs have high H_2 permeabilities (>10^5 Barrer) relative to the well-known polymers in addition to high H_2/CH_4 selectivities in the range of 1–100. Our research group performed molecular simulations for equimolar H_2/CH_4 mixtures to examine the membrane-based separation performances of 172 MOFs under industrial operating conditions, 10 bar and 298 K.[40] Adsorption data obtained from grand canonical Monte Carlo (GCMC) and diffusion data obtained from molecular dynamics (MD) simulations were used to predict gas permeabilities and selectivities of MOF membranes. This was the largest number of MOFs for which MD simulations were performed for H_2/CH_4 mixtures in the literature. Results showed that only a small number of MOF membranes is H_2 selective and diffusion selectivity for H_2 dominates the adsorption selectivity for CH_4 in these MOFs. As can be seen from this literature review, there is no high-throughput computational study that examines the membrane-based H_2/CH_4 separation potential of all existing MOFs in the literature.

The most complete collection of MOFs maintained by the Cambridge Structural Database (CSD) was recently reported.[41] We recently screened this database for adsorption-based separation of CH_4/H_2 mixtures and reported several adsorbent evaluation metrics of MOFs such as adsorption selectivity, working capacity, adsorbent performance score, sorbent selection parameter, and regenerability.[42] However, this MOF database has not been screened for any membrane-based gas separation application to date to the best of our knowledge. This type of study is strongly needed not only to see if MOF membranes can replace traditional membranes but also to provide insights into the influence of pore size, pore topology and chemistry of MOFs on the membranes' performances. In this work, we performed the first high-throughput molecular simulation study in the literature to assess the potential of the most complete collection of MOFs for membrane-based H_2/CH_4 separation. Combining GCMC and MD simulations, we computed adsorption and diffusion coefficients of H_2 and CH_4 in all MOFs. This data was then used to estimate adsorption selectivity, diffusion selectivity and membrane selectivity of MOFs and relations between these selectivities were discussed to understand the individual effects of adsorption and diffusion on the membranes' performances. H_2/CH_4 selectivities and H_2 permeabilities of 4240 different MOF membranes were calculated and compared with traditional membranes, such as zeolites and polymers, to reveal the membrane-based H_2/CH_4 separation potential of the MOF structures. The most promising MOF membranes that are above the Robeson's upper bound[43] were identified. Mixture GCMC and MD simulations were also performed for the top ten most promising MOF membranes to evaluate their performances for separation of equimolar H_2/CH_4 mixtures under practical operating conditions. Results were compared with the predictions of molecular simulations performed at infinite dilution loadings of single-component gases. The accuracy of the high-throughput screening of MOFs based on single-component adsorption and diffusion data was discussed in detail. We finally examined the relations between structural properties of MOFs such as pore sizes, porosities, surface areas, densities, lattice structure types, metal types and their membrane selectivities and gas permeabilities

to provide quantitative structure–performance relationships that can serve as a map for the development of new MOF membranes with better H_2/CH_4 separation performances. This type of fundamental understanding into structure–performance relations of MOF membranes that are capable of achieving energy efficient H_2/CH_4 separations has the potential to allow revolutionary changes in practical gas separation applications. Therefore, results presented in this work, identification of the high performance MOF membranes and microscopic insights provided for the structure–performance relations, will motivate a large number of researchers working on design and development of MOF membranes for various gas separations.

2. Computational methods

2.1 MOFs

The most complete collection of MOFs and the only collection integrated within the CSD database generated by Jimenez's group[41] was used in this work. This collection is comprised of 54 808 non-disordered MOFs with a wide range of chemical and structural properties. We first removed the bound and unbound solvents in MOFs using a Python script available in the literature[41] and then computed structural properties of MOFs such as pore limiting diameter (PLD), the largest cavity diameter (LCD), accessible gravimetric surface area (SA), porosity (ϕ) and density (ρ) using Zeo++ software.[44] We refined the MOF database to remove the materials that have zero accessible gravimetric SAs. In order to compute gas permeabilities through the MOF membranes, gas diffusivities should be computable within the pores of MOFs. The kinetic diameters of H_2 (2.96 Å) and CH_4 (3.73 Å) are different leading to different diffusion rates. We focused on the MOFs that have PLDs greater than 3.8 Å so that both CH_4 and H_2 molecules can pass through the membranes' pores. As a result of these refinements, we ended up with 4240 different MOFs that span a wide range of chemical and structural functionalities. In order to investigate structural similarities of MOFs, a similarity matrix was built following the algorithms described in the literature.[45,46] Each MOF structure was used as a seed one by one and compared to all MOFs using constrained ray trace method. In order to provide high statistical accuracy, 100 000 sample points with 0.5 Å probe size was provided into the Zeo++ software. Peak height ratios between different ray trace intensities were summed and normalized with the total data points to create a similarity index. Similarity index between 0 and 1 provides a range of similarity measure for MOF structures, 0 as the least similar and 1 as the most similar.

2.2 Molecular simulations

GCMC and MD simulations, which have been widely used to compute gas adsorption isotherms and diffusivities in porous materials,[47] were performed in this work as implemented in the RASPA simulation code.[48] The gas–gas and gas-MOF interactions were defined using Lennard-Jones (LJ) potential. Single-site spherical LJ 12–6 potential was used to model H_2 (ref. 49) and CH_4 (ref. 50) molecules. The potential parameters of MOF atoms were taken from the Universal Force Field (UFF).[51] These force fields were selected based on the results of our previous simulation studies in which very good agreements between our simulations and experimental measurements were shown for CH_4 and H_2 uptakes[38,52,53] and diffusivities[54] in many MOFs. The validity of our computational approach to predict the membrane performances of various MOFs (such as IRMOF-1, ZIF-8, ZIF-69, ZIF-78, ZIF-90, ZIF-95, Ni-MOF-74, $Zn(bdc)(ted)_{0.5}$) was also shown in several of our previous studies[40,55,56] in which good agreements between our simulations and experiments for single-component H_2 and CH_4 permeabilities and for equimolar H_2/CH_4 mixture permeabilities were reported.

The Henry's constants (K^0) of gas molecules were initially calculated at the limit of zero-coverage (infinite dilution) using 10^5 moves of the Widom particle insertion method[47] by performing Monte Carlo simulations. We also performed GCMC simulations for equimolar H_2/CH_4 mixtures at 1 bar and 298 K. In mixture GCMC simulations, four different types of moves including translation, reinsertion, swap of a molecule and identity exchange of molecules were considered. The Lorentz–Berthelot mixing rules were employed and the Peng–Robinson equation of state was used to convert the pressure to the corresponding fugacity. The cut-off distance for truncation of the intermolecular interactions was set to 13 Å. The simulation cell lengths were increased to at least 26 Å along each dimension and periodic boundary conditions were applied in all simulations. For each MOF, simulations were carried out for 10 000 cycles with the first 5000 cycles for initialization and the last 5000 cycles for taking ensemble averages.

We then performed MD simulations to compute single component self-diffusivities (D^0) of H_2 and CH_4 in MOFs' pores at 298 K and infinite dilution. Following the literature,[29] we switched off the gas–gas intermolecular interactions and inserted 30 gas molecules into each MOF to represent the infinite dilution condition and to obtain high accuracy in the simulations. The self-diffusion coefficients were calculated by using the slope of the mean square displacement of gas molecules. For each MOF, MD simulations were carried out for 10^6 cycles in the NVT ensemble using a time step of 1 fs. We used 1000 initialization cycles and 10 000 equilibration cycles. The Nosé–Hoover thermostat[47] was used in NVT-MD simulations. We also performed mixture MD simulations and the initial states of these simulations were created with the appropriate loadings determined from the GCMC simulations performed at 1 bar and 298 K. Both gas–gas and gas–framework interactions were considered. Mixture MD simulations were carried out using 10^6 cycles in the NVT ensemble with a time step of 1 fs. At least 10 trajectories were used to compute self-diffusivities of each component. More details of these simulations can be found in the literature.[47,57]

MOFs were assumed to be rigid in their reported crystallographic structures in simulations. This assumption has been used in all large-scale molecular simulation studies of MOFs to save significant computational time. We recently showed that if the MOF has large pore sizes, framework flexibility has a negligible effect on the gas permeability and H_2/CH_4 selectivity of MOF membranes.[40] Flexibility was found to affect only gas

permeability without changing the selectivity of the MOF membranes which have narrow pore sizes. In this work, we only considered MOFs with pore sizes larger than the kinetic diameters of both gas molecules, therefore flexibility is expected to have a negligible effect on the results.

2.3 High-throughput screening methodology

It is important to differentiate the methodology of our current work from our previous work. In our previous work,[42] we performed GCMC simulations for equimolar CH_4/H_2 mixtures and reported adsorption selectivities of MOFs at 1 and 10 bar. In this work, we used a different approach to model MOF membranes: we first computed the Henry's constants (K^0) of gas molecules at infinite dilution using the Widom particle insertion method and then performed MD simulations to compute single component self-diffusivities (D^0) again at infinite dilution for all 4240 MOFs. Using this information, adsorption selectivities, diffusion selectivities and membrane selectivities of MOFs ($S^0_{ads,CH_4/H_2}$, $S^0_{diff,\ H_2/CH_4}$, and $S^0_{mem,H_2/CH_4}$) were computed in addition to the gas permeabilities ($P^0_{H_2}$ and $P^0_{CH_4}$) as described in the equations given in Table 1. We then identified the promising MOF membranes, which have membrane selectivities, $S^0_{mem,H_2/CH_4}$ greater than 10 and H_2 permeabilities, $P^0_{H_2}$ greater than 10^4 Barrer. Mixture GCMC and MD simulations were only performed for the top ten most promising MOF membranes that have the highest $S^0_{mem,H_2/CH_4}$ because performing MD simulations for gas mixtures is computationally very demanding due to the very large number of gas molecules interacting with each other and with the MOF atoms. These MD simulations were performed considering equimolar H_2/CH_4 mixtures at 1 bar and 298 K. Calculations of mixture membrane selectivities ($S^{mix}_{mem,H_2/CH_4}$) and mixture gas permeabilities ($P^{mix}_{H_2}$ and $P^{mix}_{CH_4}$) are also shown in Table 1. It is important to note that our suggested computational approach makes accurate predictions for the separation performances of MOF membranes. Fig. 1 shows the comparison of our results with the experimentally reported data for single-component CH_4 and H_2 permeances and H_2/CH_4 mixture permeances of several fabricated MOF membranes including IRMOF-1, Ni-MOF-74, ZIF-8, ZIF-69, ZIF-78, ZIF-90, ZIF-95. We also presented the good agreement between our calculations and experiments for the gas permeabilities of CH_4 and H_2 through mixed matrix membranes having MOFs (IRMOF-1 and CuBTC) as fillers in Fig. S1.† Gas permeance measurement conditions and related experimental references of MOF membranes and MOF-based mixed matrix membranes can be seen in Table S1.† All these results validate the accuracy of our computational approach.

Table 1 Calculated membrane properties of MOFs[a]

	Formula
Permeability	$P^0_i = K^0_i \times D^0_i$
Adsorption selectivity	$S^0_{ads,i/j} = \frac{K^0_i}{K^0_j}$
Diffusion selectivity	$S^0_{diff,i/j} = \frac{D^0_i}{D^0_j}$
Membrane selectivity	$S^0_{mem,i/j} = S^0_{ads,i/j} \times S^0_{diff,i/j}$
Mixture adsorption selectivity	$S^{mix}_{ads,i/j} = \frac{C_i}{C_j} \Big/ \frac{y_i}{y_j}$
Mixture diffusion selectivity	$S^{mix}_{diff,i/j} = \frac{D^{mix}_i}{D^{mix}_j}$
Mixture membrane selectivity	$S^{mix}_{mem,i/j} = S^{mix}_{ads,i/j} \times S^{mix}_{diff,i/j}$

[a] K^0: Henry's constant at infinite dilution. D^0: self-diffusivity at infinite dilution. C: loading of the gas species in the mixture. y: composition of the gas species in the bulk phase. D^{mix}: self-diffusivity of gas species in the mixture. i, j: gas species and i/j represents the selectivity of i over j.

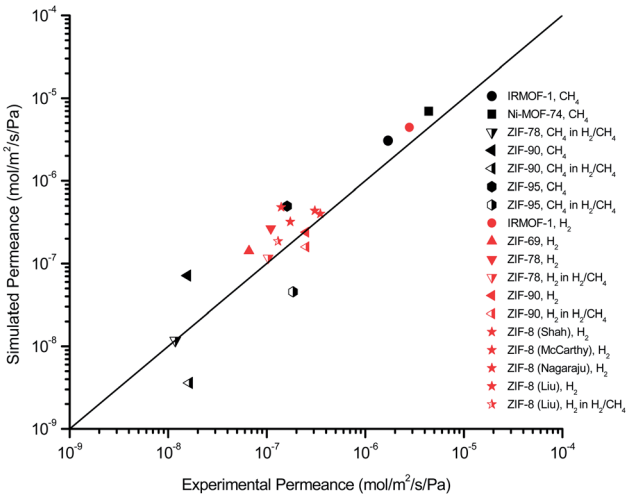

Fig. 1 Comparison of our results and experiments for single-component and mixture gas permeances through IRMOF-1, Ni-MOF-74, ZIF-8, ZIF-69, ZIF-78, ZIF-90 and ZIF-95 membranes. Gas permeance measurement conditions of MOF membranes and related experimental references can be seen in Table S1.†

3. Result and discussions

3.1 Performances of MOF membranes

Selectivity has been considered as the most critical factor to assess both equilibrium and kinetic-based separation potentials of materials. Adsorption selectivity is used to evaluate MOF adsorbents and membrane selectivity is used to assess MOF membranes, which is calculated as the multiplication of adsorption and diffusion selectivities as shown in Table 1. We first compared these three selectivities to understand the influence of adsorption and diffusion on the performance of MOF membranes in Fig. 2. CH_4 is energetically preferred over H_2 and it is more strongly adsorbed compared to H_2 in all MOFs. The K^0 values of CH_4 and H_2 were calculated to be in the range of 1.36×10^{-7}–8.27×10^{-4} mol kg^{-1} Pa^{-1} and 1.97×10^{-8}–1.89×10^{-6} mol kg^{-1} Pa^{-1}, respectively. Since $K^0_{CH_4}$ is larger than $K^0_{H_2}$ in all MOFs, adsorption selectivity favors CH_4 over H_2. Adsorption selectivities of MOFs for CH_4 over H_2 computed at infinite dilution loading ($S^0_{ads,CH_4/H_2}$) range from 1.40 to 5.68×10^3. Since the aim of this work is to identify the MOF membranes that are H_2 selective, we defined all three

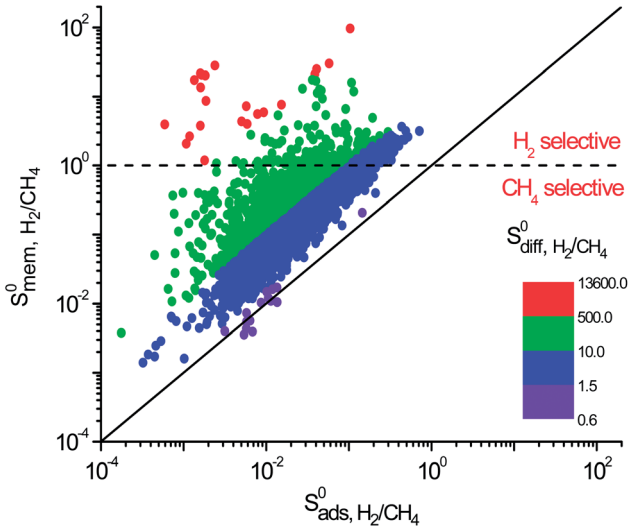

Fig. 2 Adsorption, diffusion and membrane selectivities of MOFs calculated for H_2/CH_4 separation at 298 K. The diagonal line is given to guide the eye, the dashed line shows the gas preference of the membrane.

selectivities as H_2/CH_4. Therefore, $S^0_{ads,H_2/CH_4}$ values are less than 1 on the x axis of Fig. 2. Diffusion favors H_2 over CH_4 because lighter, smaller and weakly adsorbed H_2 molecules diffuse faster than the heavier, bulkier and strongly adsorbed CH_4 molecules. The self-diffusivities of CH_4 and H_2 ($D^0_{CH_4}$ and $D^0_{H_2}$) in MOFs were computed to be between 1.36×10^{-8}–1.5×10^{-3} $cm^2\ s^{-1}$ and 1.8×10^{-8}–1.35×10^{-2} $cm^2\ s^{-1}$, respectively. As a result, diffusion selectivities of MOFs for H_2 over CH_4 computed at infinite dilution ($S^0_{diff,H_2/CH_4}$) range from 0.58 to 1.36×10^4. The colored dots in Fig. 2 show the distribution of $S^0_{diff,H_2/CH_4}$. There are 16 MOFs in which $S^0_{diff,H_2/CH_4}$ ranges from 0.6 to 1.5 (purple points), indicating that CH_4 diffusion is almost at the same order with the H_2 diffusion in these MOFs. A large number of MOFs (2749) has $1.5 < S^0_{diff,H_2/CH_4} < 10$ (blue points) and 1453 MOFs have high diffusion selectivities between 10 and 500 (green points). Those are the MOFs in which H_2 diffuses faster than CH_4. A smaller number of MOFs (22) exhibits very high diffusion selectivity, >500, for H_2 as shown by red points in Fig. 2.

The membrane selectivities of MOFs computed at infinite dilution ($S^0_{mem,H_2/CH_4}$) change from 1.4×10^{-3} to 97. The majority of the MOFs (3777) was identified to be CH_4 selective as shown in Fig. 2. The maximum CH_4 selectivity of MOF membranes was predicted to be 713. In these MOFs, high adsorption selectivity towards CH_4 dominates the diffusion selectivity towards H_2. We calculated selectivity of 68 MOFs to be around unity, $0.9 \leq S^0_{mem,H_2/CH_4} \leq 1$, which means they do not have a preference for CH_4 or H_2, therefore they cannot be used as selective membranes. A smaller number of MOFs, 395, was found to be H_2 selective. In these MOFs, high diffusion selectivity towards H_2 overcompensates the adsorption selectivity towards CH_4 and the highest H_2 selectivity of the MOF membrane was estimated to be 97. Overall, Fig. 2 represents that the most H_2 selective MOF membranes are the ones that have high diffusion selectivities as shown in red colors.

Separation performances of MOF membranes were compared with those of traditional polymer and zeolite membranes to assess the potential of MOFs in H_2/CH_4 separations. Polymeric membranes have been reported to be selective for H_2 over CH_4 and Robeson[43] described an upper bound for these membranes. Several polyimide membranes establish the upper bound at the low H_2 permeability end whereas poly(-trimethylsilylpropyne) membranes are located at the high H_2 permeability end of the upper bound. Fig. 3 shows H_2 permeability and H_2/CH_4 selectivities of MOF membranes together with the Robeson's upper bound. The H_2 permeabilities of MOF membranes were calculated to have a very wide range from 0.372 to 1.67×10^6 Barrer. Most of MOFs (4162) exhibit H_2 permeabilities in the range of 10^4–10^6 Barrer as shown with blue points in Fig. 3. At that point it is important to highlight the importance of studying the entire MOF database rather than focusing on a small number of MOFs having similar physical and chemical properties. In our previous work,[40] by studying 172 MOFs, we concluded that H_2 permeabilities of MOFs are generally in the range of 10^3–10^5 Barrer. In this work, by examining the most recent and complete collection of the MOF database that spans a large variety in pore sizes and chemical topologies, we showed that H_2 permeabilities of many MOFs are actually very large, $>10^5$ Barrer. Since these H_2 permeabilities are significantly higher than the permeabilities of polymeric membranes, we extrapolated the Robeson's upper bound with a dashed line in Fig. 3. High gas permeabilities of MOFs can be attributed to their high porosities as we will discuss below. 1545 MOFs were found to exceed the upper bound either due to their high H_2 permeabilities or high H_2 selectivities or a combination of these two. In order to describe the most promising membrane materials, we specifically focused on the MOFs that have $S^0_{mem,H_2/CH_4} \geq 10$ and $P^0_{H_2} > 10^4$ Barrer, which are shown by red points in Fig. 3. Gas diffusivities, gas permeabilities, adsorption, diffusion and membrane selectivities of the top ten MOF membranes are all listed in Table 2 in addition to their structural properties.

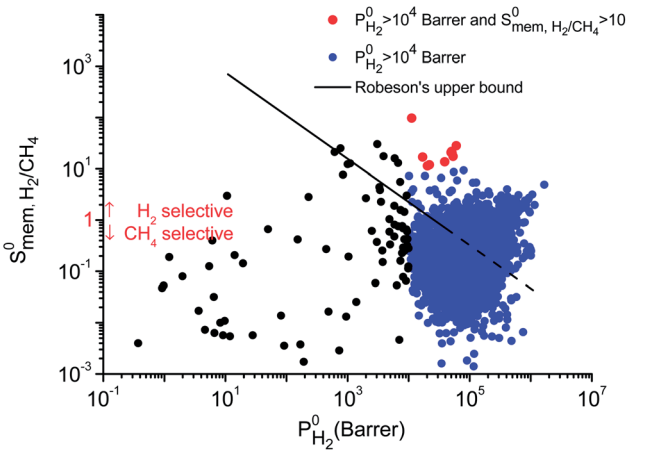

Fig. 3 Selectivity and permeability of MOF membranes computed at infinite dilution at 298 K. The black solid line represents the Robeson's upper bound for H_2/CH_4 separation performance of the polymeric membranes.

Table 2 Performances of the top 10 MOF membranes computed at infinite dilution, 298 K

MOF	LCD (Å)	PLD (Å)	ϕ	$D^0_{CH_4}$ (cm^2 s^{-1})	$D^0_{H_2}$ (cm^2 s^{-1})	$P^0_{CH_4}$ (Barrer)	$P^0_{H_2}$ (Barrer)	$S^0_{ads,CH_4/H_2}$	$S^0_{diff,H_2/CH_4}$	$S^0_{mem,H_2/CH_4}$
MEFMEQ	5.24	4.26	0.52	2.98×10^{-7}	2.77×10^{-4}	1.16×10^{2}	1.13×10^{4}	9.60	930.57	96.95
OGAJEN	6.47	3.96	0.55	3.74×10^{-8}	4.36×10^{-4}	2.15×10^{3}	6.02×10^{4}	416.16	11 650.87	28.00
OGAMOA	6.37	3.80	0.54	2.58×10^{-8}	3.51×10^{-4}	2.33×10^{3}	5.06×10^{4}	626.72	13 599.93	21.70
OGALEP	6.38	3.80	0.54	2.78×10^{-8}	3.49×10^{-4}	2.38×10^{3}	4.96×10^{4}	603.51	12 558.17	20.81
OGALUF	6.38	3.84	0.54	3.35×10^{-8}	3.68×10^{-4}	2.56×10^{3}	5.17×10^{4}	545.05	10 995.69	20.17
OGAKUE	6.32	3.81	0.54	2.82×10^{-8}	3.63×10^{-4}	3.09×10^{3}	5.37×10^{4}	743.25	12 896.03	17.35
PIZHOX	6.01	4.81	0.65	5.58×10^{-7}	2.36×10^{-4}	1.01×10^{3}	1.70×10^{4}	24.99	422.00	16.88
OGAJAJ	6.24	3.82	0.54	3.22×10^{-8}	2.72×10^{-4}	2.87×10^{3}	3.89×10^{4}	622.61	8438.47	13.55
HIFVUO	7.50	5.98	0.71	4.50×10^{-6}	4.65×10^{-4}	1.84×10^{3}	2.18×10^{4}	8.67	103.15	11.90
QONKOV	5.98	4.81	0.64	1.01×10^{-6}	2.74×10^{-4}	1.80×10^{3}	2.04×10^{4}	24.09	272.50	11.31

The most promising MOF membrane in Table 2 is MEFMEQ. This MOF offers both high $P^0_{H_2}$, 1.1×10^4 Barrer and high $S^0_{mem,H_2/CH_4}$, 97. The high membrane selectivity is due to its large diffusion selectivity towards H_2 (931) that dominates the weak adsorption selectivity towards CH_4 (9.6). Similarly, the second most promising MOF, OGAJEN, has a high $S^0_{mem,H_2/CH_4}$ (28) due to its high diffusion selectivity for H_2 (11 651). Although adsorption strongly favored CH_4 in this MOF with a selectivity of 416, very fast diffusion of H_2 (4.4×10^{-4} cm^2 s^{-1}) compared to CH_4 (3.7×10^{-8} cm^2 s^{-1}) dominated the adsorption selectivity. In fact, Table 2 shows that all promising MOF membranes have very high $S^0_{diff,H_2/CH_4}$ (>100). These MOFs have narrow PLDs, generally around 3.8–4.8 Å, close to the kinetic diameter of CH_4. Strongly confined CH_4 molecules diffuse slowly, in the order of 10^{-6}–10^{-8} cm^2 s^{-1}, in these MOFs whereas H_2 diffusion is at least two orders of magnitude higher, 10^{-4} cm^2 s^{-1}. As a result of this difference in diffusivities, MOFs become H_2 selective membranes. Relations between selectivities and structural properties of MOFs will be discussed in detail below.

We also compared the MOF membranes with zeolite membranes. Similar to polymeric membranes, zeolites CHA, LTA and ITQ-29 (which is the pure silica version of LTA, in other words, the same structure) are H_2 selective membranes because they have narrow windows which are not accessible for CH_4 molecules. H_2 selectivities of these zeolite membranes were reported as ~89, 17, 125 and their H_2 permeabilities were reported as 4.57×10^4, 5.8×10^3 and 8.21×10^3 Barrer, respectively.[58] MOFs offer similar H_2 selectivities and higher H_2 permeabilities than these zeolites. Zeolite MFI, which has larger pore windows compared to other zeolites, was reported to exhibit high CH_4 permeability (~10^5 Barrer) and it is a CH_4 selective membrane with a selectivity of 13. We identified 795 MOF membranes that are much more CH_4 selective ($S^0_{mem,CH_4/H_2}$ in the range of 13–713) and much more CH_4 permeable ($P^0_{CH_4}$ in the range of 1.0×10^5–1.2×10^8 Barrer) than MFI membrane. Carbon nanotube membranes (CNT) were shown to exhibit very large CH_4 permeabilities (2×10^7 Barrer) and good CH_4 selectivities (28) due to the very fast diffusion of gas molecules (0.1–1 cm^2 s^{-1}) which was attributed to the smoothness of the potential energy surface.[59] 17 MOFs were identified to outperform CNT membranes in terms of CH_4 selectivities (69–713) and CH_4 permeabilities (~10^7–10^8 Barrer) in this work. This comparison shows that several MOFs can replace or even outperform zeolite and polymer membranes in H_2/CH_4 separations.

Results obtained so far showed that there are many promising MOFs that offer high permeability and selectivity for efficient separation of H_2 from CH_4. However, these MOFs have not been fabricated as membranes so far. In other words, MOFs that we identified as top promising membranes have not been fabricated as membranes yet, therefore it is not possible to make a direct comparison between experiments and simulations for the top promising MOF membranes. We already showed the good agreement between our simulations and experimental measurements for the performance of several different types of fabricated, prototype MOF membranes in Fig. 1 and we believe that these are the direct evidence of the good predicting power of our calculation methodology. Membrane studies in the literature generally focused on well-known MOFs. For example, several different research groups[18,19] fabricated IRMOF-1 (also known as MOF-5) membranes and reported its H_2/CH_4 selectivity as 2–3 and H_2 permeance (permeability divided by membrane thickness) as 8–47×10^{-7} mol m^{-2} s^{-1} Pa^{-1} based on single-component gas measurements. By studying the entire MOF database, we found that there are 21 MOFs that possess H_2/CH_4 selectivity >2 and H_2 permeance >50×10^{-7} mol m^{-2} s^{-1} Pa^{-1} assuming 25 μm membrane thickness. There are 39 MOFs that exhibit H_2/CH_4 selectivity around 2, similar to MOF-5. It is important to note that selectivity and permeance of the MOF-5, SAHYIK in the CSD, was predicted as 1.39 and 44×10^{-7} mol m^{-2} s^{-1} Pa^{-1} in this work which agree well with the experimentally reported values.[40,56] These results highlight the importance of computational screening of the entire MOF database to direct the experimental studies to more promising membrane materials. At that point, we would like to note that one of the most widely fabricated MOF membrane, ZIF-8, did not appear in our discussion because we limited our focus with MOFs having limiting pore sizes greater than 3.8 Å so that both CH_4 and H_2 molecules can pass through the membranes' pores. Since the small pore size of ZIF-8 was computed as 3.4 Å, this MOF was not included in the 4240 MOFs that we examined.

3.2 Structure–performance relations

Understanding the relations between structural properties and performances of MOF membranes for a target gas separation is useful not only to easily identify the promising candidates but also to guide the design and synthesis of new MOFs with exceptionally high membrane-based gas separation performances. We examined the relations between K^0 of gases, D^0 of gases, three different selectivities and structural properties of MOFs, pore sizes (PLD and LCD), surface areas (SA), porosities (ϕ) and densities (ρ). Fig. 4(a) shows that $K^0_{CH_4}$ generally decreases with increasing LCD since small cavities are more favorable adsorption sites for large CH_4 molecules due to the strong confinement. The degree of confinement of H_2 molecules in MOFs with small pores and MOFs with large pores can be thought as similar, because in both cases H_2 molecule is small relative to the pore size giving similar, low $K^0_{H_2}$ values. As a result of this, $S^0_{ads,CH_4/H_2}$ of MOFs generally decreases with LCD as shown in Fig. 4(b). Although this relation is not perfect, it is obvious that MOFs with LCDs > 12 Å exhibit lower $S^0_{ads,CH_4/H_2}$. For example, the average $S^0_{ads,CH_4/H_2}$ is about 26 for MOFs having LCD > 12 Å. Relations between K^0 of gases and other structural properties, PLD, SA, ϕ and ρ are given in Fig. S2.† $K^0_{CH_4}$ decreases with PLD and SA but there is no obvious relation between $K^0_{CH_4}$ and ϕ, ρ. As the SA and ϕ (ρ) increase (decreases), $K^0_{H_2}$ increases. Relations between $S^0_{ads,CH_4/H_2}$ and PLD, SA, ϕ, ρ are also shown in Fig. S3† and results showed that S^0_{ads} decreases (increases) with increased pore sizes, SA and ϕ (ρ).

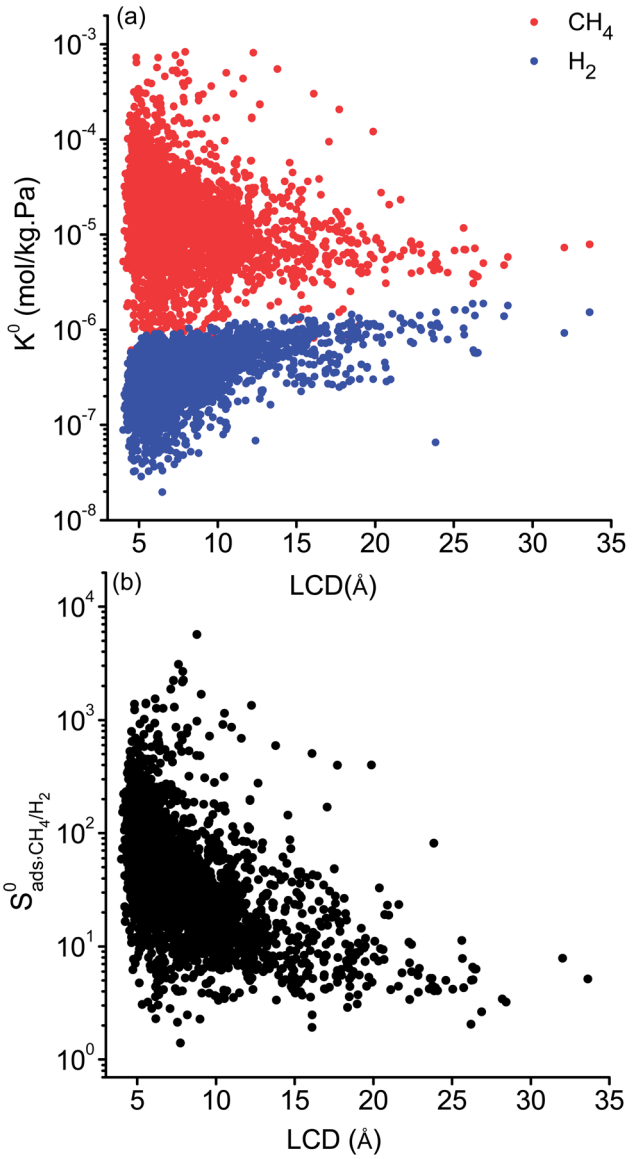

Fig. 4 (a) Henry's constants of gases (b) adsorption selectivity as a function of LCD of MOFs.

We then examined relations between gas diffusivities and PLDs of MOFs. Fig. 5(a) and (b) show that both $D^0_{CH_4}$ and $D^0_{H_2}$ increase as the PLD and ϕ of MOFs increase. $D^0_{H_2}$ is generally at least one order of magnitude larger than $D^0_{CH_4}$ in MOFs having small PLDs (<5 Å) since smaller H_2 molecules diffuse faster than the bulkier CH_4 molecules in narrow pores of MOFs. Diffusivities get close to each other in MOFs having large pore sizes (>10 Å) since both gases can easily diffuse regardless of the molecular size. As a result of these, the highest $S^0_{diff,H_2/CH_4}$ is located at PLDs < 5 Å and ϕ < 0.75 as shown in Fig. 5(c). As the PLD and ϕ increase, $S^0_{diff,H_2/CH_4}$ generally decreases since both molecules can readily diffuse regardless of their molecular sizes. At that point it is important to note that diffusion rates of gases and hence S^0_{diff} do not solely depend on the kinetic diameters of gas molecules and pore sizes of MOFs. At the narrow PLD region, $D^0_{CH_4}$ and $D^0_{H_2}$ show a large variety of values from 10^{-8} to 10^{-3} $cm^2\ s^{-1}$ indicating that diffusion is not only determined by the pore sizes but also interactions between gas molecules and MOFs play an important role. Finally, Fig. S4† shows that D^0 of both gases generally increases (decreases) with increased SA and ϕ (ρ). This is expected because as the porosity increases, framework density decreases and gas molecules easily diffuse in less confined spaces. Since both diffusivities have similar trends with the SA and ρ, $S^0_{diff,H_2/CH_4}$, which was calculated as the ratio of diffusivity of H_2 to that of CH_4, is almost independent from them. According to Fig. S5,† S^0_{diff} does not show an obvious dependency to SA, ϕ, and ρ. Relations between P^0 of gases, PLD and ϕ of MOFs are shown in Fig. 6. The trend of P^0 and PLD shown in Fig. 6(a) is very similar to the one between D^0 and PLD given in Fig. 5(a), since $D^0_{H_2}$ increases with ϕ, $P^0_{H_2}$ also increases. Fig. S6† represents that $P^0_{H_2}$ is positively (negatively) correlated with SA (ρ) due to the same reasons we discussed for $D^0_{H_2}$. As a result of these, narrow pore sizes and smaller porosities lead to higher $S^0_{mem,H_2/CH_4}$ as shown in Fig. 6(c). $S^0_{mem,H_2/CH_4}$ also shows an increasing (decreasing) trend with respect to SA and ϕ (ρ) as shown in Fig. S7.† We defined quantitative limits for the structural properties of MOFs that lead to high performance membranes in the next section. It is also important to note that these structure–performance relations have some similarities with the ones reported in a molecular simulation study which examined the CO_2/CH_4 separation performances of hypothetical MOF membranes that have PLDs between 3 and 4 Å.[29] It was shown that diffusivities of CO_2 and CH_4 increase with increasing PLDs of hypothetical MOFs and the highest diffusion selectivities for CO_2/CH_4 were obtained at the low PLD region, between 3.0 and 3.2 Å. In our work, we considered real,

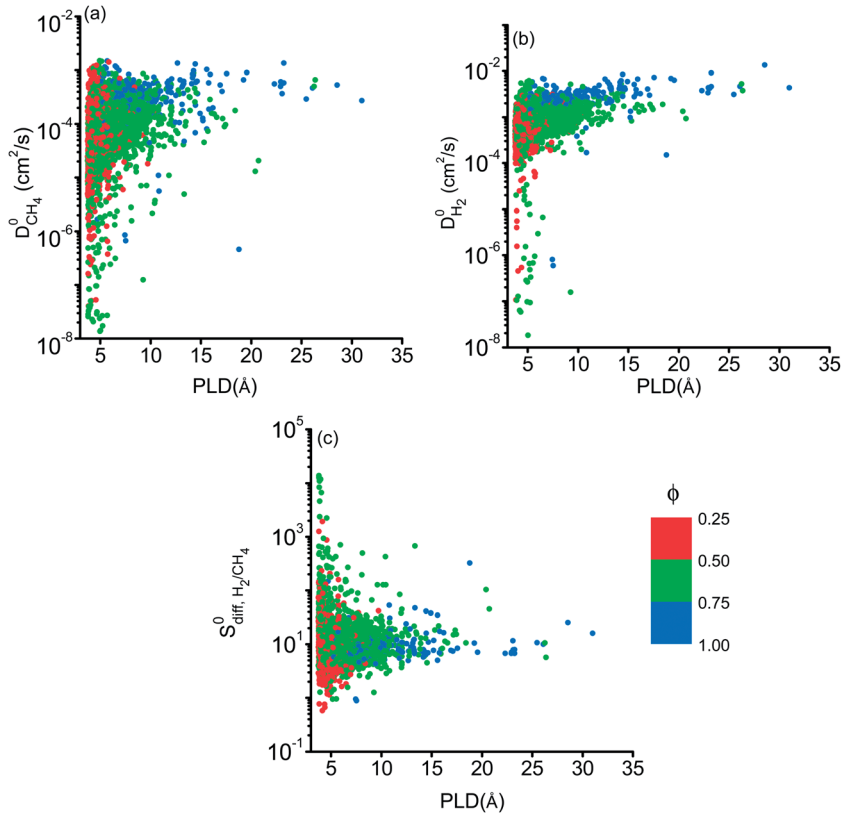

Fig. 5 Self diffusivities of (a) CH_4 (b) H_2 as a function of PLDs of MOFs. (c) Diffusion selectivities of MOFs for H_2/CH_4 as a function of PLD and porosity.

synthesized MOF database with PLDs between 3.8 and 31 Å and showed that the highest diffusion selectivities for H_2/CH_4 separation was also found to be at the low PLD region, <5 Å.

3.3 Top promising MOF membranes

So far, we examined the structure–performance relations for the entire MOF database. We now turn to the top ten promising MOFs that offer the highest $S^0_{mem,H_2/CH_4}$. The aim is to provide better understandings of the fundamental physics behind the most promising MOF membranes at the molecular level in order to facilitate rational design of new materials. This structure–performance analysis will also guide the experimental studies to select MOFs with pre-determined structural characteristics in order to achieve high performance H_2/CH_4 separation. Fig. 7 shows the effects of PLD, LCD, the ratio of PLD to LCD, SA, ϕ, ρ, lattice system and metal types available in the MOFs on the H_2 selectivities of the MOF membranes. The outer circle represents all MOFs considered in this study (4240 MOFs), the middle circle represents the top 100 H_2 selective MOFs with $P^0_{H_2} > 10^4$ Barrer and the inner circle represents the top 10 most promising MOFs that we discussed in Table 2, the ones having $S^0_{mem,H_2/CH_4} > 10$ and $P^0_{H_2} > 10^4$ Barrer. This analysis suggests that MOFs with 3.8 Å < PLD < 6 Å, 6 Å < LCD < 12 Å, SA < 1000 m^2 g^{-1}, 0.5 < ϕ < 0.75, 1 < ρ < 1.5 g cm^{-3} are the most promising membranes. This analysis also suggests that triclinic and monoclinic MOFs are more promising for H_2/CH_4 separations compared to other lattice types. MOFs have a large variety of metals in their structures but most MOFs have Ag, Cd, Cu, Co, Zn. The top ten MOF membranes generally have Cd, Cu and Zn and more specifically, monoclinic MOFs having Cu metals were found to be promising as H_2 selective membranes.

We also examined the structural similarities of the top ten most promising MOFs and results are shown in Fig. S8† together with the 2 × 2 × 2 unit cell representations of these MOFs. Structural similarity between two MOFs is represented with an index. Green colors correspond to the most similar materials, the ones having similarity index >0.8. Light green colors represent highly similar structures with indexes between 0.7 and 0.8, yellow colors show the slightly similar structures with indexes between 0.5 and 0.7 and orange colors correspond to least similar structures with indexes between 0.3 and 0.5. Red colors show the dissimilar MOFs in term of their analyzed ray trace representation resulting in an index of 0.0–0.3. Fig. S8† shows that MEFMEQ and 6 OGA-materials have high similarities with indexes greater than 0.8. PIZHOX and QONKOV also showed similarities with other top MOFs with an index of 0.65 whereas the index between those two structures was 0.83 indicating a high similarity. HIFVUO has the least similarity with other MOFs giving indexes around 0.5. There is no red color in Fig. S8† which means that the top ten MOF membranes have some common structural features which is also observable from the unit cell representations.

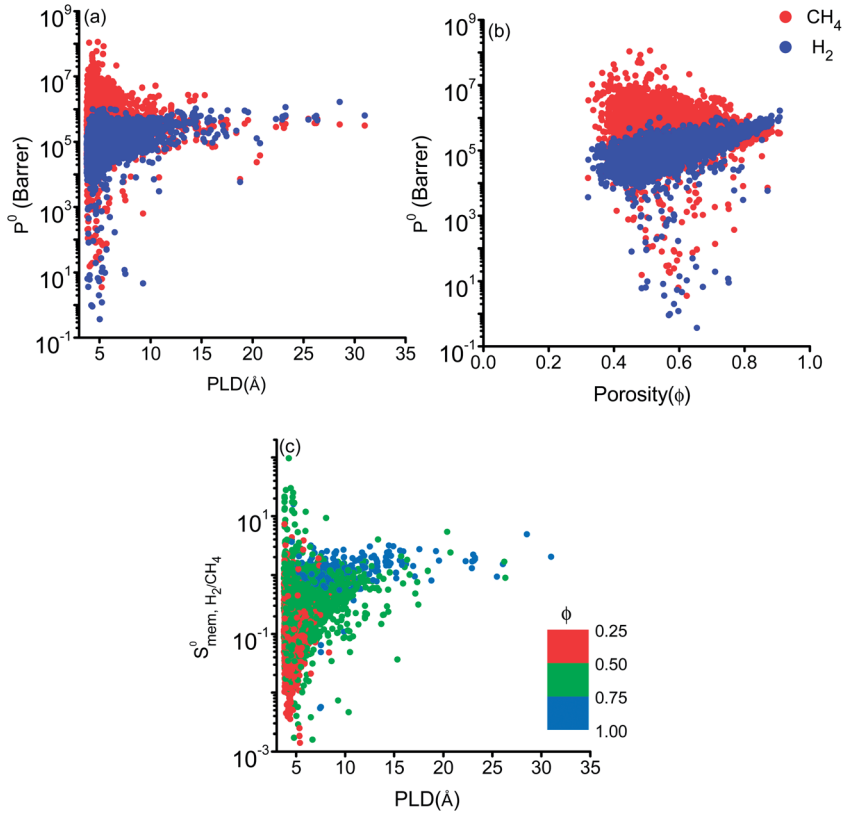

Fig. 6 Gas permeabilities as a function of (a) PLD (b) porosity of MOFs. (c) Membrane selectivities of MOFs for H_2/CH_4 as a function of PLD and porosity.

As explained in the screening strategy described in Section 2.3, the top ten most promising MOFs were identified by performing single-component simulations at infinite dilution. We also performed equimolar mixture GCMC and MD simulations at 1 bar to unlock the mixture separation performances of the top promising MOF membranes under realistic operating conditions. Gas diffusivities, permeabilities, and all three selectivities computed using single-component data at infinite dilution were compared with the ones computed for equimolar mixtures in Table 3. Results showed that mixture adsorption selectivities are similar to the ones computed at infinite dilution for 4 MOFs, HIFVUO, MEFMEQ, PIZHOX and QONKOV. These are the MOFs that have relatively low adsorption selectivities, <25. On the other hand, the MOFs (OGA-materials) which exhibit very high adsorption selectivities at infinite dilution, ~500, were found to have significantly lower mixture adsorption selectivities, ~90. Fig. S9† compares $S^{mix}_{ads,CH_4/H_2}$ computed at 1 bar with $S^{0}_{ads,CH_4/H_2}$ for the entire MOF database and results show that infinite dilution adsorption selectivities significantly overestimate mixture adsorption selectivities especially if the MOF is highly CH_4 selective (>50). For 4 MOFs which have similar $S^{mix}_{ads,CH_4/H_2}$ and $S^{0}_{ads,CH_4/H_2}$ (MEFMEQ, PIZHOX, HIFVUO and QONKOV), mixture gas diffusivities were found to be very similar to the ones computed at infinite dilution. As a result, membrane selectivity computed for mixture ($S^{mix}_{mem,H_2/CH_4}$) was found be close to the membrane selectivity computed at infinite dilution ($S^{0}_{mem,H_2/CH_4}$). On the other hand, for MOFs that have significant differences between $S^{0}_{ads,CH_4/H_2}$ and $S^{mix}_{ads,CH_4/H_2}$, mixture diffusivities were computed to be different than the single-component diffusivities. Table 3 shows that $D^{mix}_{CH_4}$ is almost one order of magnitude larger than $D^{0}_{CH_4}$ whereas $D^{mix}_{H_2}$ and $D^{0}_{H_2}$ are almost same. The increase in the diffusion rate of CH_4 can be attributed to the multi-component mixture effects[60] and collaborative interactions between many adsorbed CH_4 molecules, which are missing in the single-component case. It is known that fast-diffusing gas molecules (in our case H_2) can fasten the slow-diffusing gas molecules (in our case CH_4) in the MOFs' pores due to the multi-component mixture effects.[36] As a result, $S^{mix}_{diff,H_2/CH_4}$ becomes much lower than $S^{0}_{diff,H_2/CH_4}$. Overall, simulations performed for equimolar mixtures at 1 bar give higher adsorption selectivities but lower diffusion selectivities for H_2 than the simulations performed at infinite dilution. As a result, H_2 selectivities of MOF membranes, which were computed as the multiplication of adsorption and diffusion selectivities, become similar. Comparison of the single-component and mixture calculations for the H_2 permeability and H_2/CH_4 selectivities of the top promising MOF membranes is also given in Fig. S10.† 9 out of 10 top performing MOFs analyzed using mixture simulations still satisfy the two performance criteria, $S^{0}_{mem,H_2/CH_4} > 10$ and $P^{0}_{H_2} > 10^4$ Barrer, used to identify the best MOF membranes. This result shows that the high-throughput computational screening strategy which utilizes gas loadings and diffusivities computed at infinite dilution can be used to make quick and accurate estimations for

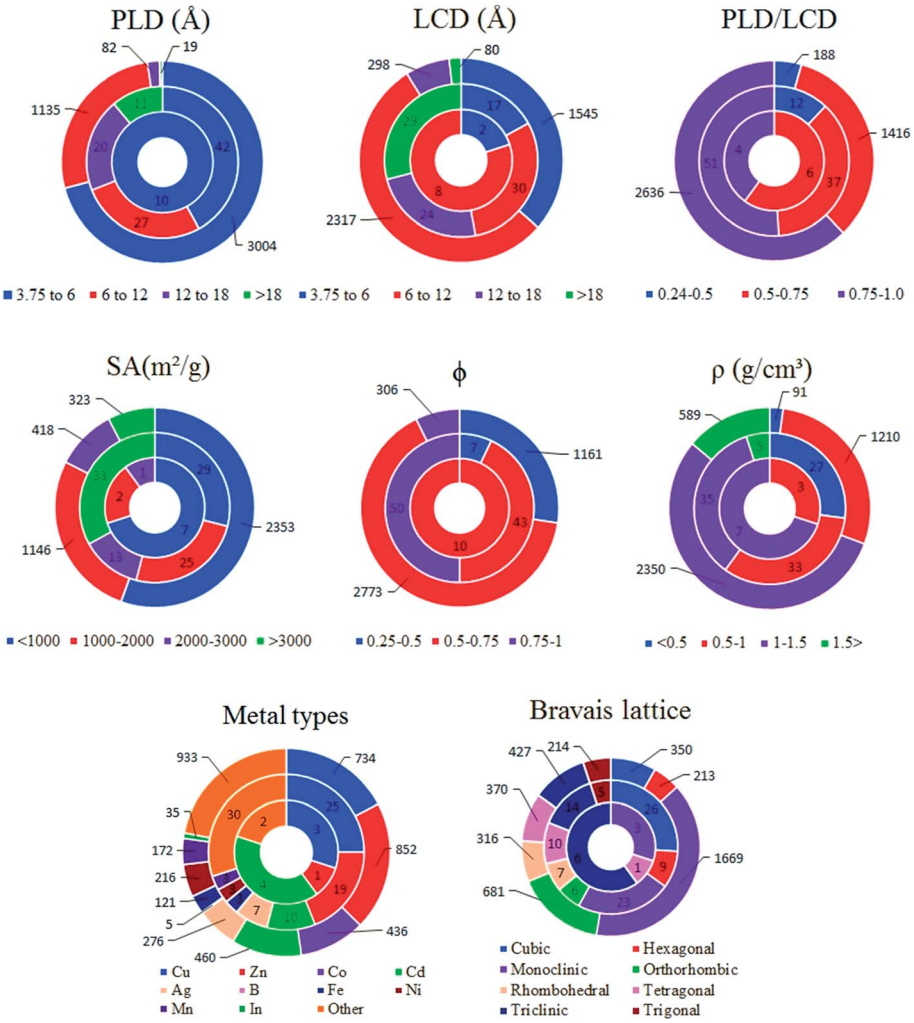

Fig. 7 Effects of structural properties on the performance of MOF membranes. Numbers on the circles represent the number of MOFs. The outer circle represents all MOFs considered in this study (4240 MOFs), the middle circle represents the top 100 H_2 selective MOFs having $P^0_{H_2} > 10^4$ Barrer and the inner circle represents the top 10 most promising MOFs that we discussed in Table 2, the ones having $S^0_{mem,H_2/CH_4} > 10$ and $P^0_{H_2} > 10^4$ Barrer.

the mixture separation performances of MOF membranes to identify the most promising candidates.

Finally, it is important to discuss the advancement of this work compared to our previous study on MOF membranes.[40] In our previous work, we performed mixture GCMC and MD simulations to predict membrane performances of 172 types of MOFs. In this work, we described a high-throughput computational screening strategy which utilizes gas loadings and diffusivities computed at infinite dilution to make accurate estimations for the mixture separation performances of MOF membranes. Since we screened a very large number of MOF membranes, we were able to show clear structure–performance results that were not present when we studied only hundreds of MOFs. Therefore, we advanced the methodology to save significant computational time and also provided solid insights into structure–performance relations of MOFs by studying the whole MOF database.

4. Conclusion

High-throughput computational screening of the MOF database was performed combining GCMC and MD simulations to examine membrane-based H_2/CH_4 separation performances of MOFs. Adsorption, diffusion and membrane selectivities of 4240 MOFs were computed at infinite dilution. Results showed that there are more than 1500 MOFs which exhibit high H_2 selectivity or high H_2 permeability or both. Many MOF membranes were identified to outperform polymer and zeolite membranes in H_2/CH_4 separations by exceeding the upper bound. The top ten most promising MOF membranes were identified and gas permeabilities and selectivities of these membranes were also calculated for separation of equimolar H_2/CH_4 mixtures using GCMC and MD simulations. Results obtained from the mixture simulations were found to be similar to the results obtained from the single-component gas simulations, indicating that high-throughput computational

Table 3 Comparison of MOF membranes' performances computed using single-component data at infinite dilution and mixture data at 1 bar, 298 K

MOF	$S^{0}_{ads,CH_4/H_2}$	$S^{mix}_{ads,CH_4/H_2}$	$S^{0}_{diff,H_2/CH_4}$	$S^{mix}_{diff,H_2/CH_4}$	$S^{0}_{mem,H_2/CH_4}$	$S^{mix}_{mem,H_2/CH_4}$	$D^{0}_{CH_4}$ (cm^2 s^{-1})	$D^{mix}_{CH_4}$ (cm^2 s^{-1})	$D^{0}_{H_2}$ (cm^2 s^{-1})	$D^{mix}_{H_2}$ (cm^2 s^{-1})
MEFMEQ	9.60	10.01	930.57	526.66	96.95	52.60	2.98×10^{-7}	3.86×10^{-7}	2.77×10^{-4}	2.04×10^{-4}
OGAJEN	416.16	86.74	11 650.87	1700.71	28.00	19.61	3.74×10^{-8}	2.63×10^{-7}	4.36×10^{-4}	4.47×10^{-4}
OGAMOA	626.72	90.95	13 599.93	1527.64	21.70	16.80	2.58×10^{-8}	2.30×10^{-7}	3.51×10^{-4}	3.51×10^{-4}
OGALEP	603.51	91.19	12 558.17	1408.20	20.81	15.44	2.78×10^{-8}	2.74×10^{-7}	3.49×10^{-4}	3.86×10^{-4}
OGALUF	545.05	93.86	10 995.69	2068.35	20.17	22.04	3.35×10^{-8}	2.30×10^{-7}	3.68×10^{-4}	4.76×10^{-4}
OGAKUE	743.25	96.23	12 896.03	1969.58	17.35	20.47	2.82×10^{-8}	1.96×10^{-7}	3.63×10^{-4}	3.85×10^{-4}
PIZHOX	24.99	23.72	422.00	567.13	16.88	23.91	5.58×10^{-7}	4.70×10^{-7}	2.36×10^{-4}	2.66×10^{-4}
OGAJAJ	622.61	97.36	8438.47	1800.22	13.55	18.49	3.22×10^{-8}	1.77×10^{-7}	2.72×10^{-4}	3.19×10^{-4}
HIFVUO	8.67	8.31	103.15	171.90	11.90	20.68	4.50×10^{-6}	3.76×10^{-6}	4.65×10^{-4}	6.44×10^{-4}
QONKOV	24.09	22.93	272.50	251.49	11.31	10.97	1.01×10^{-6}	9.49×10^{-7}	2.74×10^{-4}	2.39×10^{-4}

screening strategy which uses gas loadings and diffusivities computed at infinite dilution can be used to make rapid and accurate estimations for the mixture separation performances of MOF membranes. We performed structure–performance analysis for the MOF membranes and results showed that MOFs with 3.8 Å < PLD < 6 Å, 6 Å < LCD < 12 Å, SA < 1000 m^2 g^{-1}, 0.5 < ϕ < 0.75, 1 < ρ < 1.5 g cm^{-3} are the most promising MOF membranes exhibiting $P^{0}_{H_2} > 10^4$ Barrer and $S^{0}_{mem,H_2/CH_4} > 10$. These promising MOFs generally have Cd, Cu and Zn as their metals. The top ten most promising MOFs were found to have common structural features based on similarity index analysis. The MOFs identified as top promising membranes have not been fabricated as membranes yet, therefore it is not possible to make a direct comparison between experiments and simulations for these membranes. We already showed the good agreement between our simulations and experimental measurements for the performance of several different types of fabricated, prototype MOF membranes and we believe that these are the direct evidence of the good predicting power of our calculation methodology. Our results will be useful to guide the experimental synthesis of new MOF membranes to achieve high performance H_2/CH_4 separations and the computational methodology employed in this work will be used to identify the promising MOF membranes for various industrially important gas separations.

Conflicts of interest

There are no conflicts of interest to declare.

Acknowledgements

S. K. acknowledges ERC-2017-Starting Grant. This study has received funding from the European Research Council (ERC) under the European Union's Horizon 2020 research and innovation programme (ERC-2017-Starting Grant, grant agreement No. 756489-COSMOS).

References

1 M. Eddaoudi, H. Li and O. Yaghi, *J. Am. Chem. Soc.*, 2000, **122**, 1391–1397.
2 O. M. Yaghi, M. O'Keeffe, N. W. Ockwig, H. K. Chae, M. Eddaoudi and J. Kim, *Nature*, 2003, **423**, 705–714.
3 N. Stock and S. Biswas, *Chem. Rev.*, 2011, **112**, 933–969.
4 V. Guillerm, D. Kim, J. F. Eubank, R. Luebke, X. Liu, K. Adil, M. S. Lah and M. Eddaoudi, *Chem. Soc. Rev.*, 2014, **43**, 6141–6172.
5 Y. Basdogan and S. Keskin, *CrystEngComm*, 2015, **17**, 261–275.
6 S. Keskin, T. M. Van Heest and D. S. Sholl, *ChemSusChem*, 2010, **3**, 879–891.
7 L. B. Li, R. B. Lin, R. Krishna, X. Q. Wang, B. Li, H. Wu, J. P. Li, W. Zhou and B. L. Chen, *J. Mater. Chem. A*, 2017, **5**, 18984–18988.
8 J. Della Rocca, D. Liu and W. Lin, *Acc. Chem. Res.*, 2011, **44**, 957–968.
9 R. J. Kuppler, D. J. Timmons, Q.-R. Fang, J.-R. Li, T. A. Makal, M. D. Young, D. Yuan, D. Zhao, W. Zhuang and H.-C. Zhou, *Coord. Chem. Rev.*, 2009, **253**, 3042–3066.
10 H. Furukawa, K. E. Cordova, M. O'Keeffe and O. M. Yaghi, *Science*, 2013, **341**, 1230444–1230456.
11 J.-R. Li, J. Sculley and H.-C. Zhou, *Chem. Rev.*, 2011, **112**, 869–932.
12 M. Shah, M. C. McCarthy, S. Sachdeva, A. K. Lee and H. K. Jeong, *Ind. Eng. Chem. Res.*, 2012, **51**, 2179–2199.
13 E. Adatoz, A. K. Avci and S. Keskin, *Sep. Purif. Technol.*, 2015, **152**, 207–237.
14 S. L. Qiu, M. Xue and G. S. Zhu, *Chem. Soc. Rev.*, 2014, **43**, 6116–6140.
15 A. Kasik and Y. S. Lin, *Sep. Purif. Technol.*, 2014, **121**, 38–45.
16 Z. X. Zhao, X. L. Ma, A. Kasik, Z. Li and Y. S. Lin, *Ind. Eng. Chem. Res.*, 2013, **52**, 1102–1108.
17 Z. X. Zhao, X. L. Ma, Z. Li and Y. S. Lin, *J. Membr. Sci.*, 2011, **382**, 82–90.
18 Y. Yoo, Z. P. Lai and H. K. Jeong, *Microporous Mesoporous Mater.*, 2009, **123**, 100–106.
19 Y. Y. Liu, Z. F. Ng, E. A. Khan, H. K. Jeong, C. B. Ching and Z. P. Lai, *Microporous Mesoporous Mater.*, 2009, **118**, 296–301.
20 Y. Y. Mao, W. Cao, J. W. Li, Y. Liu, Y. L. Ying, L. W. Sun and X. S. Peng, *J. Mater. Chem. A*, 2013, **1**, 11711–11716.
21 J. P. Nan, X. L. Dong, W. J. Wang, W. Q. Jin and N. P. Xu, *Langmuir*, 2011, **27**, 4309–4312.

22 V. V. Guerrero, Y. Yoo, M. C. McCarthy and H. K. Jeong, *J. Mater. Chem.*, 2010, **20**, 3938–3943.
23 D. F. Liu, X. L. Ma, H. X. Xi and Y. S. Lin, *J. Membr. Sci.*, 2014, **451**, 85–93.
24 M. Shah, H. T. Kwon, V. Tran, S. Sachdeva and H. K. Jeong, *Microporous Mesoporous Mater.*, 2013, **165**, 63–69.
25 Y. C. Pan, B. Wang and Z. P. Lai, *J. Membr. Sci.*, 2012, **421**, 292–298.
26 F. H. Allen, *Acta Crystallogr., Sect. B: Struct. Sci.*, 2002, **58**, 380–388.
27 R. Krishna and J. M. van Baten, *Phys. Chem. Chem. Phys.*, 2011, **13**, 10593–10616.
28 Z. W. Qiao, K. Zhang and J. W. Jiang, *J. Mater. Chem. A*, 2016, **4**, 2105–2114.
29 Z. W. Qiao, C. W. Peng, J. Zhou and J. W. Jiang, *J. Mater. Chem. A*, 2016, **4**, 15904–15912.
30 T. Watanabe and D. S. Sholl, *Langmuir*, 2012, **28**, 14114–14128.
31 M. Hong, S. Li, J. L. Falconer and R. D. Noble, *J. Membr. Sci.*, 2008, **307**, 277–283.
32 S. Adhikari and S. Fernando, *Ind. Eng. Chem. Res.*, 2006, **45**, 875–881.
33 Q. P. Yang, L. J. Li, W. Q. Tan, Y. J. Sun, H. L. Wang, J. P. Ma and X. B. Zhao, *Chem. Commun.*, 2017, **53**, 9797–9800.
34 S. Keskin and D. S. Sholl, *Langmuir*, 2009, **25**, 11786–11795.
35 S. Keskin, *Ind. Eng. Chem. Res.*, 2010, **49**, 11689–11696.
36 S. Keskin, *J. Phys. Chem. C*, 2012, **116**, 1772–1779.
37 G. Yilmaz, A. Ozcan and S. Keskin, *Mol. Simul.*, 2015, **41**, 713–726.
38 T. N. Ozturk and S. Keskin, *J. Phys. Chem. C*, 2014, **118**, 13988–13997.
39 E. Haldoupis, S. Nair and D. S. Sholl, *J. Am. Chem. Soc.*, 2010, **132**, 7528–7539.
40 I. Erucar and S. Keskin, *J. Membr. Sci.*, 2016, **514**, 313–321.
41 P. Z. Moghadam, A. Li, S. B. Wiggin, A. Tao, A. G. P. Maloney, P. A. Wood, S. C. Ward and D. Fairen-Jimenez, *Chem. Mater.*, 2017, **29**, 2618–2625.
42 C. Altintas, I. Erucar and S. Keskin, *ACS Appl. Mater. Interfaces*, 2018, **10**, 3668–3679.
43 L. M. Robeson, *J. Membr. Sci.*, 2008, **320**, 390–400.
44 T. F. Willems, C. H. Rycroft, M. Kazi, J. C. Meza and M. Haranczyk, *Microporous Mesoporous Mater.*, 2012, **149**, 134–141.
45 M. Pinheiro, R. L. Martin, C. H. Rycroft, A. Jones, E. Iglesia and M. Haranczyk, *J. Mol. Graphics Modell.*, 2013, **44**, 208–219.
46 R. L. Martin, B. Smit and M. Haranczyk, *J. Chem. Inf. Model.*, 2012, **52**, 308–318.
47 D. Frenkel and B. Smit, *Understanding Molecular Simulation: From Algorithms to Applications*, Academic Press, San Diego, 2nd edn, 2002.
48 D. Dubbeldam, S. Calero, D. E. Ellis and R. Q. Snurr, *Mol. Simul.*, 2016, **42**, 81–101.
49 V. Buch, *J. Chem. Phys.*, 1994, **100**, 7610–7629.
50 M. G. Martin and J. I. Siepmann, *J. Phys. Chem. B*, 1998, **102**, 2569–2577.
51 A. K. Rappe, C. J. Casewit, K. S. Colwell, W. A. Goddard and W. M. Skiff, *J. Am. Chem. Soc.*, 1992, **114**, 10024–10035.
52 T. N. Ozturk and S. Keskin, *Ind. Eng. Chem. Res.*, 2013, **52**, 17627–17639.
53 K. B. Sezginel, A. Uzun and S. Keskin, *Chem. Eng. Sci.*, 2015, **124**, 125–134.
54 C. Altintas and S. Keskin, *RSC Adv.*, 2017, **7**, 52283–52295.
55 Y. Basdogan, K. B. Sezginel and S. Keskin, *Ind. Eng. Chem. Res.*, 2015, **54**, 8479–8491.
56 E. Adatoz and S. Keskin, *J. Nanomater.*, 2015, **2015**, 1–9.
57 D. Dubbeldam, A. Torres-Knoop and K. S. Walton, *Mol. Simul.*, 2013, **39**, 1253–1292.
58 R. Krishna and J. M. van Baten, *J. Membr. Sci.*, 2010, **360**, 323–333.
59 H. Chen and D. S. Sholl, *J. Membr. Sci.*, 2006, **269**, 152–160.
60 J. C. Liu, S. Keskin, D. S. Sholl and J. K. Johnson, *J. Phys. Chem. C*, 2011, **115**, 12560–12566.